An efficient renewable hybridization based on hydrogen storage for peak demand reduction

A rule-based energy control and optimization using machine learning techniques

Behzadi, Amirmohammad; Alirahmi, Seyed Mojtaba; Yu, Haoshui; Sadrizadeh, Sasan

Published in:
Journal of Energy Storage

DOI (link to publication from Publisher):
10.1016/j.est.2022.106168

Publication date:
2023

Document Version
Publisher's PDF, also known as Version of record

Journal of Energy Storage 57 (2023) 106168

Contents lists available at ScienceDirect

Journal of Energy Storage

journal homepage: www.elsevier.com/locate/est

Research papers

An efficient renewable hybridization based on hydrogen storage for peak demand reduction: A rule-based energy control and optimization using machine learning techniques

Amirmohammad Behzadi [a,*], Seyed Mojtaba Alirahmi [b], Haoshui Yu [b], Sasan Sadrizadeh [a,c]

[a] Department of Civil and Architectural Engineering, KTH Royal Institute of Technology, Stockholm, Sweden
[b] Department of Chemistry and Bioscience, Aalborg University, Esbjerg, Denmark
[c] School of Business, Society and Engineering, Mälardalen University, Västerås, Sweden

ARTICLE INFO

Keywords:
Hydrogen storage
Thermal energy storage
Multi-objective optimization
Energy management
Fuel cell
Solar collector

ABSTRACT

The present study proposes and thoroughly examines a novel approach for the effective hybridization of solar and wind sources based on hydrogen storage to increase grid stability and lower peak load. The parabolic trough collector, vanadium chloride thermochemical cycle, hydrogen storage tank, alkaline fuel cells, thermal energy storage, and absorption chiller make up the suggested smart system. Additionally, the proposed system includes a wind turbine to power the electrolyzer unit and minimize the size of the solar system. A rule-based control technique establishes an intelligent two-way connection with energy networks to compensate for the energy expenses throughout the year. The transient system simulation (TRNSYS) tool and the engineering equation solver program are used to conduct a comprehensive techno-economic-environmental assessment of a Swedish residential building. A four-objective optimization utilizing MATLAB based on the grey wolf algorithm coupled with an artificial neural network is used to determine the best trade-off between the indicators. According to the results, the primary energy saving, carbon dioxide reduction rate, overall cost, and purchased energy are 80.6 %, 219 %, 14.8 $/h, and 24.9 MWh at optimal conditions. From the scatter distribution, it can be concluded that fuel cell voltage and collector length should be maintained at their lowest domain and the electrode area is an ineffective parameter. The suggested renewable-driven smart system can provide for the building's needs for 70 % of the year and sell excess production to the local energy network, making it a feasible alternative. Solar energy is far less effective in storing hydrogen over the winter than wind energy, demonstrating the benefits of combining renewable energy sources to fulfill demand. By lowering CO_2 emissions by 61,758 kg, it is predicted that the recommended smart renewable system might save 7719 $ in environmental costs, equivalent to 6.9 ha of new reforestation.

Nomenclature

A	Area (m^2)
$ACSR$	Annual cost saving rate (%)
$c_{electrcity}$	Electricity price ($)
c_{heat}	Heat price ($)
CDE	Carbon dioxide emission (kg)
$CDERR$	Carbon dioxide emission reduction rate (%)
CI_{PY}	cost indexes at the present year
CI_{RY}	cost indexes at the reference year
CRF	Capital recovery factor
$\dot{E}$	Electricity (kWh)
i	Interest rate
$\dot{m}$	Mass flow rate (kg/h)
n	Plant's operation years
$PESR$	Primary energy saving rate (%)
$\dot{Q}$	Heat (kWh)
TCR	Total cost rate ($/h)
V	Volume (m^3)
$\dot{W}$	Power (kW)
Z	The investment cost of components ($)
$\dot{Z}_k^{CI}$	Capital investment cost rate ($/hr)
$\dot{Z}_k^{OM}$	Operating and maintenance cost rate ($/hr)

* Corresponding author.
E-mail address: abehzadi@kth.se (A. Behzadi).

https://doi.org/10.1016/j.est.2022.106168
Received 6 September 2022; Received in revised form 17 November 2022; Accepted 18 November 2022
Available online 20 December 2022

Subscript and abbreviations

AC	Alternating current
AFC	Alkaline fuel cell
ANN	Artificial neural network
$CuCl_2$	Copper chlorine
DC	Direct current
EES	Engineering equation solver
EEA	European environment agency
IEA	International energy agency
$MgCl_2$	Magnesium chloride
MOGWO	Multi-objective grey wolf optimization
PTC	Parabolic trough collectors
PID	Proportional–integral–derivative
TES	Thermal energy storage
VCl_3	vanadium chloride

Greek symbols

η_E	Local plant's electrical efficiency (%)
η_{grid}	Energy transmission efficiency (%)
η_H	Local plant's heating efficiency (%)
$\lambda_{electricty}$	Carbon dioxide emission indices for electricity production (kg/MWh)
λ_{heat}	Carbon dioxide emission indices for heating production (kg/MWh)
γ	Operating and maintenance cost coefficient
τ	Model's operation hours

1. Introduction

1.1. Background

Global energy use has increased remarkably in the last decade (100 % growth between 2010 and 2020) [1]. The International Energy Agency (IEA) recently reported annual global energy use of 22,000 kWh per capita. Such growth is expected to continue due to population growth and life quality improvement [2]. Approximately 85 % of this energy is produced by fossil fuels such as coal, oil, and gas that emit greenhouse gases [3]. Renewable sources are the most effective and viable alternative for attaining large reductions in greenhouse gas emissions and dealing with the global energy demand sustainably. According to the information provided by the European Environment Agency (EEA), if renewable forms of energy had not been employed since 2005, the present value of carbon dioxide emission would have been >10 % greater [4].

1.2. Literature survey

Solar power is one of the cleanest and greenest renewable energies available [5]. Parabolic trough collectors (PTCs) are incredibly important among various solar-driven technologies because they operate at higher temperatures, leading to lower costs for hot storage systems [6]. The collector's trough design lets it gather more solar radiation compared to a flat panel [7]. The techno-economic comparison of a PTC-based combined heating and power system against solar power plants was evaluated by Wang et al. [8], reporting 9.5 % higher electricity production and 8.5 % lower energy costs. The feasibility of using PTCs as a prime mover of an ejector cooling and power system was assessed by Bechir et al. [7], considering Tunisian weather conditions. The simulation outcomes obtained by TRNSYS software resulted in 60 % higher performance efficiency than the conventional system. Kumaresan et al. [9] studied the performance evaluation of a solar power system consisting of PTC and thermal energy storage (TES) in India. They demonstrated a maximum efficiency of 63 %, which is considerable.

Hydrogen, the most abundant element in the universe, is another potential alternative to fossil fuels due to its highest energy value and a major contribution to sustainable development compared to other energy resources [10]. With increasing environmental contamination and fossil fuel depletion in recent years, hydrogen production from renewable waste heat/electricity has attracted considerable attention since it releases no greenhouse gas emissions [11]. In comparison to other recently developed methods of hydrogen generation, thermochemical water-splitting cycles outperform in terms of efficiency, cost, and environmental friendliness [12]. Numerous researchers have examined the techno-economic-environmental aspects of high-temperature solar-based thermochemical hydrogen production cycles. The potential of PTCs for hydrogen generation considering different regions of Algeria was evaluated and compared by Ouagued et al. [13]. According to their results, using a $CuCl_2$ (copper chlorine) thermochemical cycle integrated with PTC leads to annual hydrogen production of 84 tons in the south part of the country. A thermochemical hydrogen production cycle run by a high-temperature solar system was proposed by Yilmaz and Selbas [14], obtaining total performance efficiencies of 32.76 % and 34.56 %, respectively. Balta et al. [15] examined the influence of ambient conditions and main operational parameters on performance indicators of a PTC-based hydrogen production system consisting of the $MgCl_2$ (magnesium chloride) thermochemical cycle. The findings demonstrated that the $MgCl_2$ cycle has a lot of promise, with total cycle efficiencies above 50 %. Temiz and Dincer [16] studied the performance of a multi-generation system consisting of PTCs and $CuCl_2$ thermochemical hydrogen cycle. They achieved a promising payback period of 6 years for yearly hydrogen generation of 297 tons. The thermodynamic indicators of various chloride cycles were studied and compared by Balta et al. [17]. Their findings showed that the VCl_3 (vanadium chloride) cycle is the most efficient and promising method for producing hydrogen.

Although solar-driven technologies have attained an adequate level of technological maturity, there are still several obstacles to overcome, including the high investment cost and the intermittent nature of their energy production [18]. On the other hand, wind power is recognized as one of the most abundant and sustainable renewable resources widely used for domestic applications due to the low price of energy production [19]. As a result, combining solar and wind sources to generate cost-effective, clean, and reliable energy output can be a prudent approach in terms of both sources' availability. In the literature, several works have investigated the hybridization of solar-driven technologies and wind power systems for the multi-generation of hydrogen, electricity, heating, and cooling from techno-economic-environmental viewpoints. An innovative multi-generation system based on a wind turbine and high-temperature solar collector integrated with a $CuCl_2$ thermochemical hydrogen cycle was introduced and analyzed by Ishaq et al. [20], obtaining an acceptable performance efficiency of 50 %. Hasan and Genç [21] assessed the economic aspects of a hybrid solar-wind system combined with electrolyzers. According to their results, the hydrogen generation cost could be reduced by around 0.03 $\$/m^3$ by selling the surplus power to the local electricity grid. In another study, Wang et al. [22] proposed a green thermochemical hydrogen cycle based on trough collectors and wind powers and achieved an annual carbon dioxide reduction rate of 835 tons. Al-Buraiki and Al-Sharafi [23] designed a wind-solar system based on hydrogen production and consumption for Dhahran city, Saudi Arabia. According to their outcomes, the suggested system could supply the building's electricity demand independent of the electricity network with a significant carbon dioxide emission reduction of 9.6 tons for 1 year. A novel off-grid power system driven by photovoltaic panels and wind turbine charging the fuel cell for power generation and electrolyzer for hydrogen production was introduced by Wang et al. [24], obtaining >10 kW and 0.22 kg/h power and hydrogen production with the efficiency of 57 %.

Among different energy systems, fuel cells are the most effective device for converting the chemical energy of various fuels like hydrogen, natural gas, and syngas directly into useful electricity and heating in a

wide range of applications [25]. In comparison to typical combustion engines, fuel cells have reduced costs and emissions and improved dependability and overall efficiency. Alkaline fuel cells (AFCs) have several advantages over other types of hydrogen fuel cells, including the ability to operate at higher efficiencies and lower temperatures, as well as being less sensitive to fuel impurities and being well-suited to dynamic operating modes [26]. Wei et al. [27] investigated the thermodynamic aspects of adding AFCs to a combined system driven by solar panels and a wind turbine using TRNSYS software. The proposed system could produce >755 MWh of useful energy with an acceptable conversion efficiency. Li et al. [26] introduced and evaluated a novel solar-based system consisting of an AFC and an electrolyzer. They demonstrated that in addition to considerable electricity production with low exergy destruction, the waste heat of AFC could be used for the cogeneration of electricity through the Stirling engine and cooling via an absorption chiller. More recently, Wang et al. [28] presented a green and efficient system for electricity and cooling production and showed that the total efficiency of 77.5 % is attained thanks to the high hydrogen-to-electricity conversion rate and waste heat recovery from AFCs. Shen et al. [29] proposed a green and usable energy system based on hydrogen consumption/generation consisting of AFCs and an electrolyzer driven by a wind turbine. They showed that carefully balancing the quantity of electricity needed and the capacity of the AFC and wind turbine through proper sizing of the hydrogen storage tank would result in considerable primary energy savings and cost mitigation. The transient simulation of an off-grid solar-based hydrogen generation system integrated with AFCs to supply the electricity demand in northeast Indian states was investigated by Pal and Mukherjee [30]. They resulted in a low levelized electricity cost of 0.5 $/kWh, indicating the significance of efficient renewable integration.

In addition to integrating renewable energy-driven devices efficiently, and implementing performance improvement techniques, optimizing the energy system is critical for attaining sustainability, enhanced performance, and low cost [31,32]. Izadi et al. [33] optimized a hybrid solar-wind system comprising a wind turbine, fuel cell, and PV panels for the cogeneration of electricity and hydrogen. They revealed that finding a proper tank size through a neural network-genetic algorithm approach results in considerable power loss and carbon dioxide emission mitigations. Mehrpooya et al. [34] applied a genetic algorithm-based multi-objective optimization to find the best operating condition of a CHP system driven by PTC. Thanks to the optimization, they obtained a higher efficiency of 19.5 % and a lower annual product cost rate of 3.8 million dollars. Sadeghi et al. [35] optimized a solar $CuCl_2$ thermochemical cycle through a non-dominated sorting genetic algorithm-II to maximize the exergy efficiency while reducing product energy costs. Lately, Alirahmi et al. [36] combined the artificial neural network and different multi-criteria optimization methods to find the best operating condition of a high-temperature solar-based hydrogen generation/storage system considering the case of Los Angeles. Their outcomes concluded that the Pareto envelope-based selection algorithm II is the best optimization approach due to the lowest product energy cost and simultaneously highest exergetic round trip efficiency. Li et al. [37] optimized a hybrid wind- and solar-based energy system by applying an implicit stochastic optimization method. According to their outcomes, net energy generated and guaranteed rate were increased by 5 % and 4 %, respectively.

On the other hand, a high computation time is one of the significant challenges of optimization problems. An artificial neural network (ANN) strategy is implemented as a form of the machine learning model to solve the problem in the shortest amount of time [38]. Balafkandeh et al. [39] designed and optimized a hydrogen generation system equipped with fuel cells. They revealed that the combination of the machine learning approach and data-driven optimization results in considerably lower running time compared to the standalone optimization. Razmi et al. [40] implemented the artificial neural network in a PTC-driven hydrogen system, resulting in decreased optimization time. Behzadi et al. [12] recently applied the machine learning technique to optimize a solar-driven hydrogen production/usage system in a lower computation time.

1.3. Scientific contribution

In spite of the significant amount of effort and work that has been put into improving renewable-based multi-generation systems, the existing body of research is still struggling with a few serious challenges. The high investment cost that building owners must bear is one of the most challenging difficulties that solar-powered building energy systems must overcome. Even though this capital returns to the owners within a short time, the initial cost remains a significant obstacle. Improving the efficiency of solar thermal systems and reducing heat loss is another critical problem that should be a top priority to lower trade barriers and improve high-quality products. In order to reduce the price of energy and boost the incentive to use renewable-driven technology, it is also necessary to implement active and passive energy enhancement approaches that are both desirable and realistic. One example of this would be making use of low-temperature waste heat. Achieving these targets will help ensure a sustainable shift to an efficiently integrated, cost-effective renewable-based energy system. The present paper introduces an innovative and fully renewable-based cooling, heating, and power system driven by a high-temperature trough collector integrated with a thermochemical hydrogen cycle. The following is a list of the article's significant contributions:

- The system is equipped with an electrolyzer unit charged by a wind turbine to produce the extra hydrogen not only to reduce the solar system size but also to supply the demand when there is no solar availability.
- An efficient hybridization of renewable energy sources (solar and wind) with hydrogen production/storage ideas is presented and thoroughly examined from techno-economic-environmental aspects to enhance grid reliability and peak load shaving.
- Carbon dioxide is eliminated by using hydrogen rather than natural gas as a fuel cell's primary energy source, making the suggested hybrid systems more environmentally friendly.
- The waste heat recovery process as a passive energy enhancement method is added by exploiting the fuel cells' extra heat to generate cooling via the absorption chiller and supply the heating demands through heat exchangers and thermal energy storage tank.
- A rule-based control strategy is established to obtain a smart two-way interaction with electricity and district heating networks to effectively reimburse energy costs over the year. By this clever interaction, the battery with a high investment cost could be eliminated, making the proposed system as inexpensive yet efficient as possible.
- An artificial neural network is used for training, and an innovative grey wolf four-objective optimization technique that has not yet been utilized in any energy system is applied to contribute to Europe's green transition in the most optimal way possible.
- In order to ensure that the results are as thorough as feasible, the practicality of the proposed system under optimal conditions is assessed for a residential building complex in Lund, which has abundant solar and wind resources in Sweden.

In essence, the comparison of the present work with the same system driven by solar and wind resources published in the literature is listed in Table 1. As indicated, the performance of the proposed model and similar systems is compared based on the energy source, useful products, modeling, controllers, optimization methods, and the number of objective functions. According to the table, none of the papers in the literature have investigated and optimized the hybridization of solar and wind resources for electricity/hydrogen/heating/cooling productions, considering four conflictive objectives. Another distinguishing

Table 1
The comparison of the present work with similar systems in the above literature.

Ref.	Source		Useful outputs	Dynamic modeling	Controller	Machine learning-assisted optimization	Number of objective functions
	Solar	Wind					
[20]	✓	✓	Electricity/hydrogen/heating	×	×	×	×
[21]	✓	✓	Electricity/hydrogen	✓	×	×	×
[22]	✓	✓	Electricity/hydrogen	×	×	×	2
[23]	✓	✓	Electricity/hydrogen	✓	×	×	1
[24]	✓	✓	Electricity/hydrogen/heating	✓	×	×	×
[27]	✓	✓	Electricity/hydrogen	✓	Traditional on/off	×	×
[28]	✓	×	Electricity/hydrogen/ heating/cooling	✓	×	×	×
[29]	×	✓	Electricity/hydrogen	✓	×	×	×
[30]	✓	✓	Electricity/hydrogen	✓	×	×	2
[33]	✓	✓	Electricity/hydrogen	✓	Traditional on/off	✓	3
[35]	✓	×	Electricity/hydrogen	×	×	✓	2
[41]	✓	×	Electricity/hydrogen	✓	×	✓	2
[37]	✓	✓	Electricity	✓	×	×	2
[12]	✓	×	Electricity/hydrogen/fresh water	✓	Traditional on/off	✓	3
[40]	✓	×	Electricity/hydrogen	✓	×	✓	3
The present work	✓	✓	Electricity/hydrogen/ heating/cooling	✓	Rule-based advanced strategy	✓	4

characteristic of the present work is establishing an optimal rule-based control strategy and machine-learning technique for cost reduction, energy saving, and running time mitigation.

2. Methodology

2.1. The proposed smart system

Fig. 1 demonstrates the schematic representation of the introduced smart multi-generation system. As depicted, the solar energy absorbed by the high-temperature trough collectors as the primary mover of the system runs the thermochemical vanadium chloride cycle for hydrogen production. In order to reduce the solar system size and provide the building demands when there is no solar radiation, the wind turbine integrated with an Alkaline electrolyzer is added for extra electricity and hydrogen generation. Monitoring the hydrogen tank capacity, the auxiliary heater mode, and building electricity needs, the controllers determine whether the electricity generated by the wind turbine should charge the electrolyzer, run the auxiliary heater, supply the demand, or be sold to the local grid. According to Fig. 1, the hydrogen stored in the tank and the air consisting of nitrogen and oxygen go into the anode and cathode to start the thermochemical reaction for electricity generation in the Alkaline fuel cell. The produced electricity could either supplies the building's demand or be sold to the local grid to compensate for the energy cost. Afterward, the waste heat of low-temperature outlet gases exiting the fuel cell is recovered in the heat exchanger to increase the cooling water temperature. Based on the cooling demand, the controller commands the flow diverter to transfer the hot water from the heat exchanger to the cooling or heating system. If there is a cooling need, the hot water drives the single-effect absorption chiller to satisfy the load.

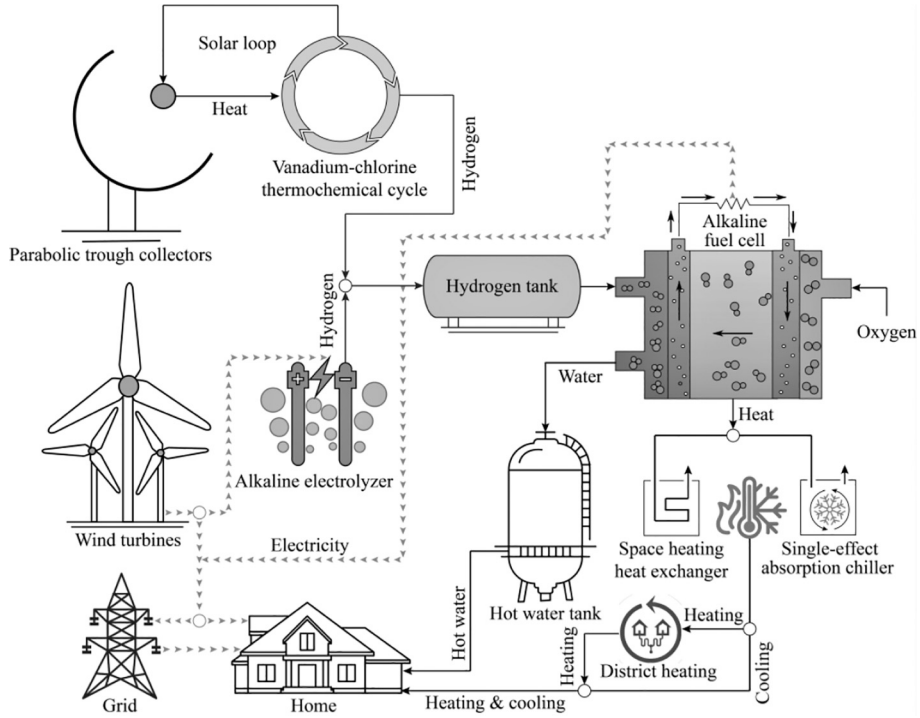

Fig. 1. Schematic representation of the studied hybrid system.

Otherwise, it goes into the botting cycle to meet the space heating or domestic hot water needs. Tracking the tank capacity and building heating demand, the controller ascertains the direction of the hot water. If the tank is not filled, the priority is to charge the tank and provide the domestic hot water need at 60 °C (assuming the case of Sweden) [42]. Otherwise, the hot water enters the space heating heat exchanger to provide the heating load or be sold to the local district heating network. In the space heating heat exchanger, the proportional–integral–derivative (PID) controller is implemented to regulate the cold side mass flow rate to obtain the supply temperature of 80 °C. As mentioned, the proposed smart system has a two-way interaction with the local energy networks. Therefore, the energy network supplies the building's demand when there is no access to renewable resources and the hydrogen tank is vacant. Also, the battery, a significant component cost, might be deleted thanks to this ingenious strategy, resulting in lower investment costs and making the owner adopt renewable-based energy systems.

2.2. The building case

The studied building is a residential multi-family apartment located in Lund in southwest Sweden, with a high abundance of solar and wind resources compared to other cities. The building consists of 10 flats with an area of 150 m^2 (10 m × 15 m) on ten floors. The heating and cooling loads are calculated using TRNBuild as a part of the TRNSYS package considering the room comfort temperature of 23 °C for all seasons. For this, the necessary information, including building characteristics, comfort criteria, hourly variation of solar radiation, ambient temperature, and wind speed, are given as input to the software. Fig. 2 illustrates Lund's hourly changes in ambient temperature over 1 year. The figure indicates that while the maximum ambient temperature reaches 26.9 °C in July (the warmest hour of 4839 h), it drops to −13.85 °C in January (the coldest hour of 281 h).

Fig. 3 illustrates the variation of solar radiation and wind speed range which are other required local information to perform the simulation and calculate the demand profiles. Fig. 3(a) shows that the maximum solar radiation (788.5 W/m^2) is attained in hour 4237 at the end of June. The figure further demonstrates that while for around 5 months of the year, the maximum hourly solar radiation is below 500 W/m^2, it reaches acceptable high values from the middle of spring to the end of summer. What stands out from Fig. 3(b) is that the wind speed varies from 0.2 m/s to 20.1 m/s. Moreover, from the average wind speed of about 7 m/s, it can be concluded that Lund has a high potential for installing wind-driven technologies since, most of the year, the wind speed is above 4 m/s.

2.3. Transient simulation

The transient simulation is conducted by linking TRNSYS with the engineering equation solver (EES) program. TRNSYS software with various components, as a potent tool for modeling smart energy systems, has been used to design and validate mathematical models for trough collectors, wind turbines, electrolyzers, fuel cells, absorption chillers, heat exchangers, and thermal energy storage tank. Since there is no component for modeling the VCl cycle in TRNSYS, the EES program with an extensive library of thermodynamics properties of various fluids is applied to compute the mass and energy balance formulations of the heat-driven hydrogen production unit. In Fig. 4, the structure of the model in the TRNSYS simulation studio is illustrated.

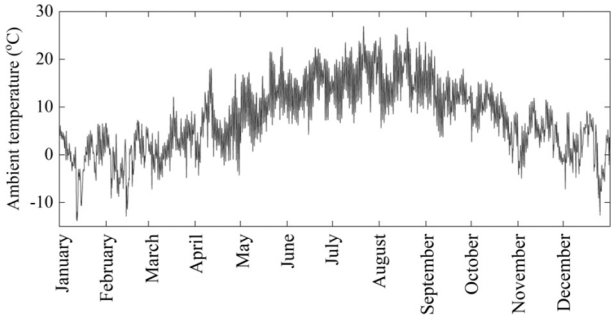

Fig. 2. The variation of ambient temperature over a year for the city of Lund.

Table 2 describes the key components and their related TRNSYS models, including trough collector, VCl cycle, electrolyzer, fuel cell, hydrogen tank, power conditioner, wind turbine, absorption chiller, and hot storage tank. Moreover, the proposed smart system has several hydraulics components comprising pumps and valves. A single-speed pump with the ability to maintain a constant outlet mass flow rate is modeled by Type 114. In this component, the maximum mass flow rate is user-specified, and the maximum electricity use is determined by an input control signal with a value that ranges from one to zero. Types 11b and 11f represent the externally controlled tempering valve and flow diverter, respectively. It is possible to control the split ratio of outlets in type 11f using an input signal as well as a set point temperature. Type 11 h is a tee piece that combines two separate water streams into a single stream. In order to establish an intelligent two-way interaction between the system and energy networks and develop a rule-based strategy, several controllers, including hydrogen, ON/OFF, and PID controllers, are used, as depicted in Fig. 4. The hydrogen controller (type 100a) is implemented to cleverly monitor and manage the integration of the wind turbine, electrolyzer, H_2 storage tank, and fuel cells as a part of an integrated mini-grid system. It is designed to work with variable power in two modes of operation. When the electrolyzer is ON, its set point power equals the maximum excess power from the wind turbine and the idle power. Otherwise, the electrolyzer is OFF, and the set point power is equal to the idle power. ON/OFF differential controllers (type 2b) create control functions with a possible value of one or zero determined by comparing the difference between upper/lower temperatures and two dead band temperature differences. At each timestep, the control function's new value is determined by the preceding timestep's input control function value. The hysteresis effect is created by connecting the controller's input control signal to its output control signal. However, hysteresis in this component can be achieved by using control signals from other components as the input controller. Besides, this controller includes a high-limit cutout for safety purposes. If the high limit condition is surpassed, the control function will be reset to zero, regardless of whether or not there is a dead band. The PID controller (type 23) is applied to determine the control signal that is necessary to keep the controlled variable at the setpoint. The tracking error and its integral and derivative affect the control signal proportionally. It is based on state-of-the-art discrete algorithms for PID controllers and implements anti-windup for the integrator.

Furthermore, Type 90 evaluates the wind turbine power output based on the power/wind speed characteristic curve provided by the manufacturers. Fig. 5 indicates the characteristic curve of a proposed wind turbine designed by the Wattuneed company and used for residential applications. According to the figure, at the speed of 13.54 m/s, the turbine power reaches the maximum value of 3500 W. The impact of air density variation and the wind speed increment with height change is also considered for turbine modeling.

Finally, since there is no component to model the vanadium chloride cycle, its thermodynamic coding should be developed in external software. Here, the thermochemical cycle's mass and energy balance equations are computed in the EES program, linked to the TRNSYS through Type 166a. According to Fig. 6, this cycle consists of three reactions at different temperatures.

According to Eq. (1), Vanadium (III) chloride is broken down into vanadium (II) chloride and chlorine gas. Eq. (2) indicates the second stage, in which the chlorine gas created in the first step combines with steam to form hydrogen chloride and oxygen gases (see Fig. 8).

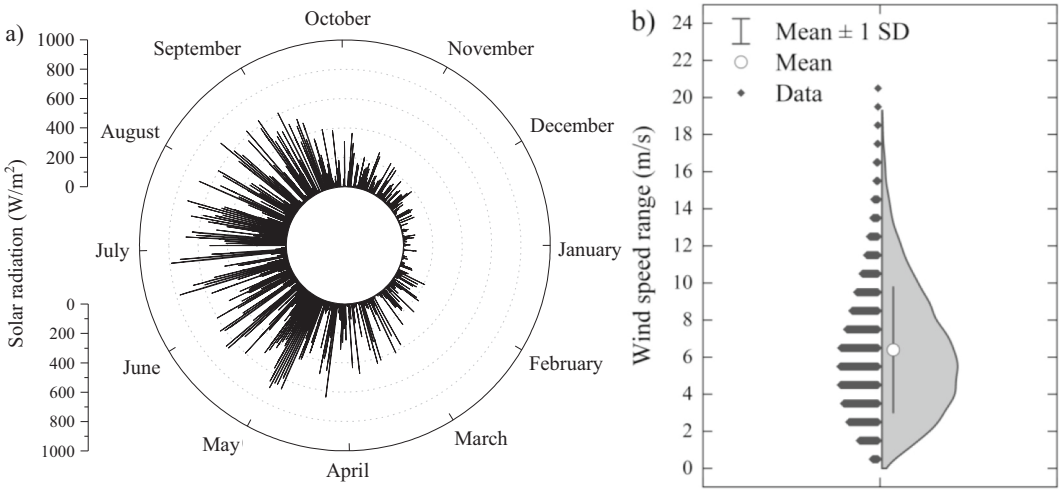

Fig. 3. The variation of a) solar radiation and b) wind speed over a year for the city of Lund.

Eventually, interactions between hydrogen chlorine gas and vanadium (II) chlorine in the solid form result in the production of hydrogen (the desirable element) and vanadium(III) chloride, as shown in Eq. (3) [12].

$$2VCl_3(s) \rightarrow 2VCl_2(s) + Cl_2(g) \tag{1}$$

$$H_2O(g) + Cl_2(g) \rightarrow 2HCl(g) + 0.5O_2(g) \tag{2}$$

$$2VCl_2(s) + 2HCl(g) \rightarrow 2VCl_3(s) + H_2(g) \tag{3}$$

Table 3 indicates the input parameters required to perform the simulation in TRNSYS. The criteria for sizing the system are to supply the average annual electricity demand of the studied building complex. In this regard, the fuel cell system is first sized to generate the maximum electricity equal to the building's average demand. Then, the size of the solar system and wind turbine is determined to produce the required hydrogen to charge the fuel cell and obtain a reasonable profile for electricity and heating production.

2.4. Techno-economic-environmental indicators

After performing a throughout transient simulation of the proposed smart system, the specific cost theory is applied to accomplish the economic assessment. Based on the concept, the costs of each component are separated into two categories: operating and maintenance and capital investment, as shown in Eq. (4) [40].

$$\dot{Z}_k = \dot{Z}_k^{OM} + \dot{Z}_k^{CI} \tag{4}$$

$$\dot{Z}_k^{OM} = \left(\frac{\gamma_k}{\tau}\right) Z_k \tag{5}$$

$$\dot{Z}_k^{CI} = \left(\frac{CRF}{\tau}\right) Z_k \tag{6}$$

$$CRF = \frac{i(1+i)^n}{(1+i)^n - 1} \tag{7}$$

where γ, τ, *CRF*, *i*, and *n* are the cost coefficient associated with the component's operating and maintenance, the model's operation hours over the year, the capital recovery factor, the interest rate, and the working years, respectively. In order to compute the component price at the present year, Marshal and Swift's correlation is implemented as indicated below [43]:

$$\dot{Z}_k^{PY} = \dot{Z}_k \times \frac{CI_{PY}}{CI_{RY}} \tag{8}$$

In this equation, CI_{PY} and CI_{RY} are the cost indexes at the present and reference years, respectively. In the present study, CI_{PY} equals 681.5, considering 2021 as the most recent year. The value/correlation of each equipment's purchased cost (Z_k) of the studied smart multi-generation system is listed in Table 4. According to the table, $\dot{W}$, *LHV*, *A*, *V*, and $\dot{Q}$ are the power production/usage, lower heating value, area, volume, and heat in kWh, kW, m^2, m^3, and kWh, respectively. Moreover, the interest rate, operating system years, and working hours are 10 %, 20, and 7446, respectively, as listed in Table 4. In the present study, the cost of replacing fuel cells is taken into account and assessed in the economic analysis. This is done assuming that fuel cells are operational for about 20,000 h.

Furthermore, as an essential economic indicator to analyze the cost-effectiveness of the proposed smart energy system, the total cost rate in $/h, which is the sum of component costs, is computed as follows:

$$TCR = \sum_{k=1}^{n_k} \dot{Z}_k \tag{9}$$

The total energies sold to and bought from the local electricity and district heating networks are calculated (Eq. (10) and Eq. (11)) to investigate the benefits of having two-way interaction with the grids to compensate for the energy costs and improve grid reliability and peak load shaving.

$$Bought\ energy = \dot{E}_{Bought} + \dot{Q}_{Bought} \tag{10}$$

$$Sold\ energy = \dot{E}_{Sold} + \dot{Q}_{Sold} \tag{11}$$

In these equations, $\dot{E}_{Bought}$ and $\dot{Q}_{Bought}$ are the electricity and heating bought from the local electricity grid and district heating network, respectively. $\dot{E}_{Sold}$ and $\dot{Q}_{Sold}$ are the electricity and heating sold to regional energy networks. Moreover, the primary energy saving rate (PESR), which is a key performance metric, is computed to investigate and compare the proposed solar- and wind-driven system against the conventional system in Sweden with separate production as follows [47]:

$$PESR = \frac{F^{Conventional} - F^{System}}{F^{Conventional}} \times 100 \tag{12}$$

$$F^{Conventional} = \frac{\dot{E}_{Demand}}{\eta_E \eta_{grid}} + \frac{\dot{Q}_{Demand}}{\eta_H \eta_{grid}} \tag{13}$$

$$F^{System} = \frac{\dot{E}_{Bought}}{\eta_E \eta_{grid}} + \frac{\dot{Q}_{Bought}}{\eta_H \eta_{grid}} - \dot{E}_{Sold} - \dot{Q}_{Sold} \tag{14}$$

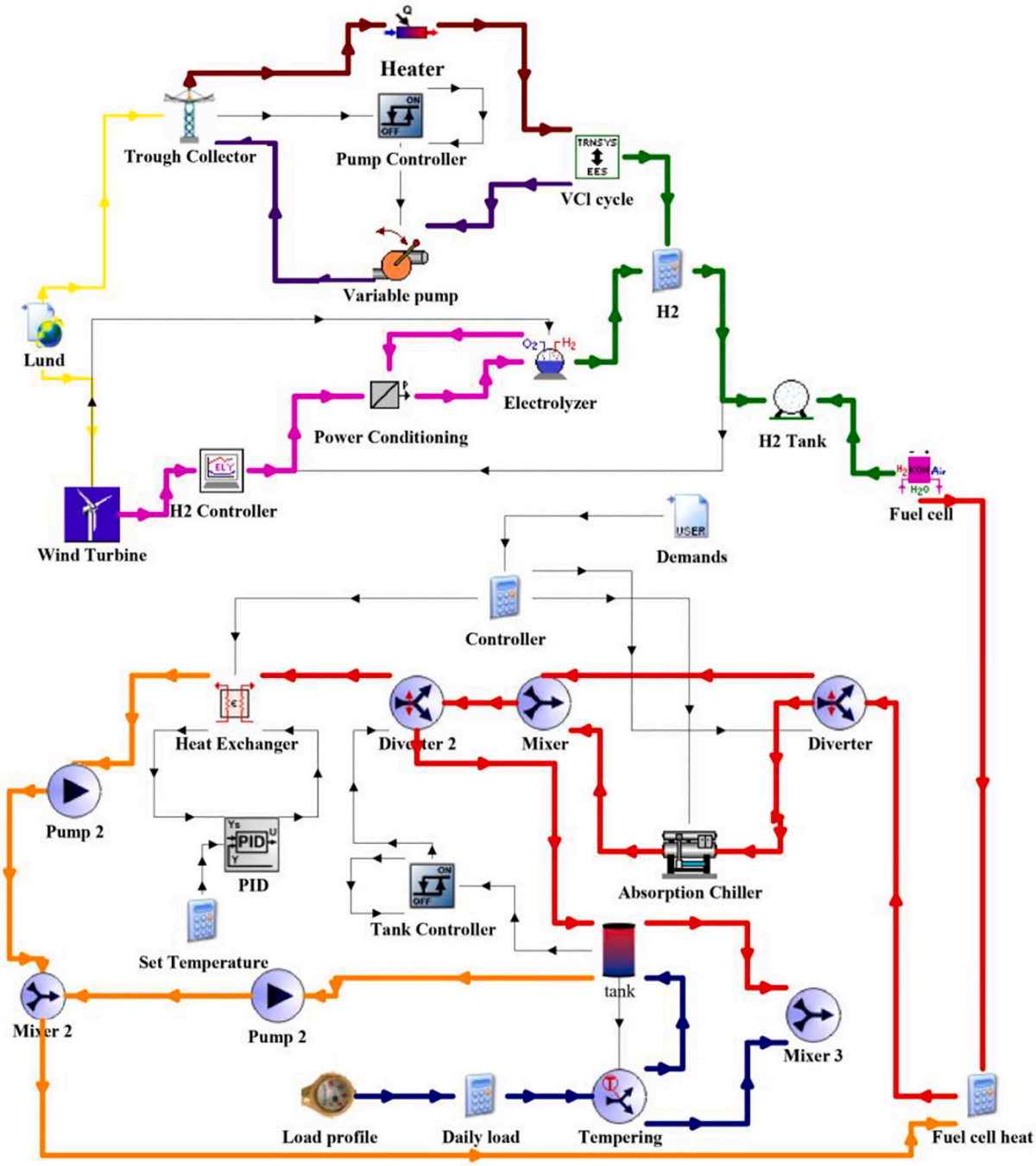

Fig. 4. The TRNSYS simulation studio project of the proposed smart multi-generation system.

where η_E, η_H, and η_{grid} are the local plant's electrical and heat efficiencies and energy transmission efficiency. After calculating each components cost and primary energy saving, the annual cost savings rate is determined to compare the proposed renewable-driven system against the reference system as follows [47]:

$$ACSR = \frac{AC^{Conventional} - AC^{System}}{AC^{Conventional}} \times 100 \quad (15)$$

$$AC^{Conventional} = \dot{E}_{Demand} \times c_{electricty} + \dot{Q}_{Demand} \times c_{heat} \quad (16)$$

$$AC^{System} = \left(\dot{E}_{Bought} - \dot{E}_{Sold}\right) \times c_{electricty} + \left(\dot{Q}_{Bought} - \dot{Q}_{Sold}\right) \times c_{heat} \quad (17)$$

In which, $c_{electrcity}$ and c_{heat} are the prices for electricity and heat in Sweden, which are 175 $/MWh and 50.72 $/MWh, respectively [48]. Eventually, environmental assessment has become more critical than ever because of the alarming increase in environmental contamination and the potentially dangerous impact of global temperature increases caused by carbon dioxide emissions. The carbon dioxide emission reduction rate (CDERR) is estimated using Eq. (18) to compare and show the effectiveness of the suggested renewable-driven building multi-generation system against traditional systems [47].

$$CDERR = \frac{CDE^{Conventional} - CDE^{System}}{CDE^{Conventional}} \times 100 \quad (18)$$

Here $CDE^{Conventional}$ and CDE^{System} are the emissions of the conventional system with the conventional system and proposed renewable-driven smart model, expressed in kilograms, and are calculated as

Table 2
The description of significant components and their corresponding model in TRNSYS.

Component	Type	Description
Trough collector	1257	Type 1257 models the parabolic trough collector with maximum compatibility for high-temperature applications. It is separated into a series of nodes analyzed based on a user-defined time step. Assuming that the high-temperature fluid is incompressible, the properties only vary with the temperature, and its effect is described as a quadratic equation. The transient equation is solved numerically for all nodes through the second-order Runge–Kutta algorithm.
Electrolyzer	160a	This type simulates the alkaline electrolyzer by applying basic thermodynamics principles, heat transfer formulas, and chemical correlations extracted experimentally. The dynamic model is calculated through a current-voltage curve as a function of temperature for a given pressure and a Faraday efficiency correlation.
Fuel cell	173a	Type 173a models a low-temperature hydrogen-fueled alkaline fuel cell with air as the cathode agent using an experimental correction for the current-voltage characteristic at the cell's operating temperature.
Hydrogen tank	164a	Type 164a simulates a compressed gas storage tank used in hydrogen storage and production systems based on the thermodynamic laws for an ideal gas.
Power conditioner	175b	This type simulates a power conditioning unit to calculate the corresponding input power considering the known output power. The model is based on experimental efficiency curves for electrically converting/inverting direct current/direct current (DC/DC) or alternating current/direct current (AC/DC).
Absorption chiller	718	Type 718 simulates a single-effect, hot water-driven absorption chiller reading catalog performance data provided by the user. Based on the present cooling capability, the machine delivers the user-specified set point temperature for the chilled water stream. The capacity is determined by the chilled water set point temperature and the temperature of the intake cooling water.
Hot storage tank	158	Type 158 represents a fluid-filled storage tank with a constant volume and vertical position. The fluid in the storage tank interacts with the surrounding environment and two flow streams that enter and exit the tank at any given time. The tank consists of isothermal temperature nodes to approximate the stratification seen in storage tanks. The user specifies the number of nodes to control the level of stratification in the tank.
Auxiliary heater	6	Type 6 simulates the electrically-driven auxiliary heater controlled either by internal or external function to raise the temperature of a stream to a user-specified value. This component operates like a furnace, generating heat at a maximum rate while keeping the outflow temperature below the set point value.
Heat exchanger	91b	Type 91b models the constant effectiveness heat exchanger. This component's maximum heat transfer is computed using the minimum capacity rate fluid and the cold and hot fluids' input temperatures independent of the system configuration.

follows:

$$CDE^{Conventional} = \dot{E}_{Demand} \times \lambda_{electricty} + \dot{Q}_{Demand} \times \lambda_{heat} \tag{19}$$

$$CDE^{Solar} = \left(\dot{E}_{Bought} - \dot{E}_{Sold}\right) \times \lambda_{electricty} + \left(\dot{Q}_{Bought} - \dot{Q}_{Sold}\right) \times \lambda_{heat} \tag{20}$$

Sweden's carbon dioxide emission indices for electricity ($\lambda_{electricty}$) and heating (λ_{heat}) are 5.1 kg/MWh and 8 kg/MWh, respectively [49].

2.5. Optimization procedure

Optimization aims to find the best possible operating conditions in terms of a set of restrictions or key parameters. In contrast to single-objective optimization, multi-objective optimization improves the concept of optimization by addressing many objectives simultaneously. Fig. 7 depicts the optimization strategy used in this study. As illustrated, TRNSYS (version 18) software and the EES (version 11.368) program are used to model the thermodynamic, economic, and environmental equations. However, since TRNSYS and EES cannot address multi-objective optimization problems, MATLAB (version 2021a) is used to implement the optimization procedure. An artificial neural network (ANN) technique is introduced to the optimization process because the coupling of TRNSYS-EES with MATLAB necessitates a considerable run time. ANN contains numerous processing elements that are inspired by the real neurons that make up the brains of mammals and birds. An ANN is a computer algorithm that relies on a network of interconnected neurons to transmit information back and forth. Because of its capacity to tackle nonlinear problems with high precision and low cost, ANN is widely used as a powerful computational method in various fields, including smart energy system optimization. The controlling mechanism used by ANNs seeks, through iterative repetition, the connections between the input, hidden, and output layers that have the greatest likelihood of success. According to Fig. 7, based on 1000 random input data points (the significant operational parameters), techno-economic-environmental analyses in TRNSYS-EES are carried out to generate the main objective functions (outputs). Subsequently, ANN with six hidden layers is used to fit the input and predict the output. This is followed by a training process determining the mathematical relationship between the design parameters and the anticipated objectives. Finally, in order to begin the optimization process, the multi-objective optimization

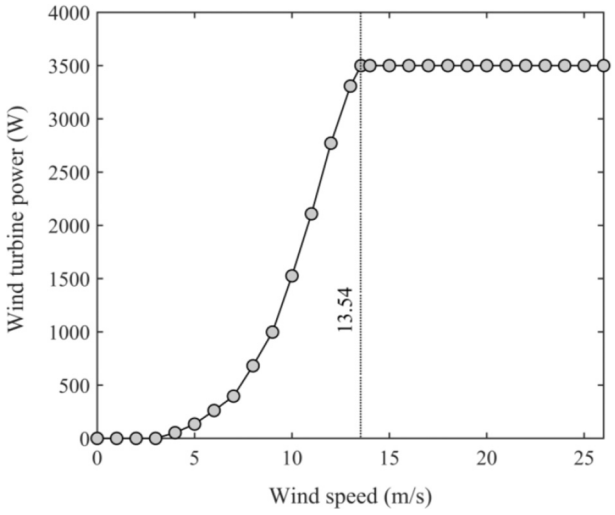

Fig. 5. The power curve of the proposed 3500 W residential wind turbine.

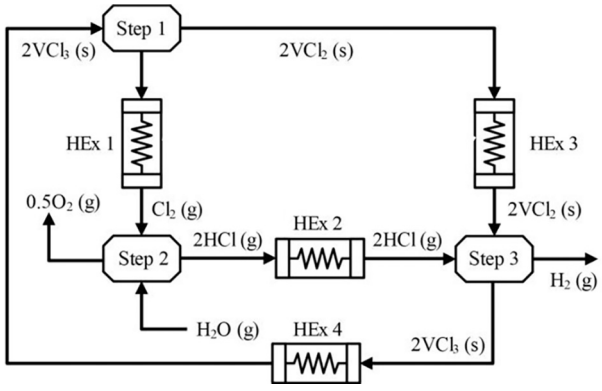

Fig. 6. The pictorial representation of chemical reactions that occurred in the VCl cycle.

Table 3
The input parameters used for the TRNSYS simulation.

Parameter	Value	Parameter	Value
Solar collector		Electrolyzer	
Collector width (m)	5	Electrode area (m^2)	0.25
Collector length (m)	38	Number of cells is series (−)	21
Inner diameter of absorber tube (m)	0.07	Number of stacks in parallel (−)	1
Focal length for collector (m)	1.8	Maximum allowable current density (mA/cm^2)	300
Mirror Accuracy (−)	0.98	Maximum allowable temperature (°C)	80
Mirro reflectivity (−)	0.93	Minimum allowable cell voltage (V)	1.4
Envelope transmittance (−)	0.96	Thermal resistance (K/W)	0.167
Absorptance of receiver coating (−)	0.95	Cooling water inlet temperature (°C)	15
Number of collectors in series (−)	0.5	Cooling water flow rate (m^3/h)	0.25
Number of collector nodes (−)	0.05	Fuel cell	
Tracking efficiency factor (−)	0.99	Number of modules in series (−)	3
Mirror cleanliness factor (−)	0.95	Number of modules in parallel (−)	2
Receiver glass dusting factor (−)	098	Electrode area (cm^2)	1000
Bellows shading factor (−)	0.97	Faraday efficiency (−)	0.987
Miscellaneous efficiency factor (−)	0.96	Fuel cell voltage (V)	5.6
Wind turbine		Ohmic resistance (ohm)	0.0116
Site elevation (m)	86	Minimum allowable cell voltage (V)	0.1
Hub height (m)	46	Fuel cell current (A)	401
Number of the turbine (−)	2	Hydrogen tank	
Site shear exponent (−)	0.14	Tank volume (m^3)	70
Thermal energy storage		Maximum allowable pressure (bar)	500
Tank volume (m^3)	3	Initial pressure level (−)	0.8
Tank height (m)	1.8	Absorption chiller	
Number of tank nodes (−)	6	Design capacity (kW)	7
Top loss coefficient (W/(m^2K)	0.7	Chilled water inlet temperature (°C)	12.2
Edge loss coefficient (W/(m^2K)	0.7	Cooling water inlet temperature (°C)	29.4
Bottom loss coefficient (W/(m^2K)	0.7	Condensate outlet temperature (°C)	75
Fluid thermal conductivity (W/(mK)	0.62	Chilled water set point (°C)	6.6

algorithm receives the extracted training network as a fitness function.

The multi-objective grey wolf optimization (MOGWO) algorithm is applied to find the best sizing of the components considering four conflictive objectives simultaneously. These include minimizing the undesirable techno-economic metrics like the bought energy and total cost rate while maximizing the favorable performance and environmental indicators such as primary energy saving and carbon dioxide emission reduction rates. The main design parameters for optimization and their domain are as follows:

$300 < \textit{fuel cell current}\ (A) < 500.$
$30 < \textit{collector length}\ (m) < 45.$
$40 < H_2\ \textit{tank volume}\ (m^3) < 70.$
5<fuel cell voltage (V)<7.5
0.65<Electrolyzer electrode area (m^2)<0.95

The cooperative nature of grey wolves during the hunting process inspired the MOGWO technique as a powerful optimization tool. MOGWO beats other multi-objective approaches regarding techno-economic aspects, such as reliability, convergence, lower processing costs, and spacing. Recent research by Behzadi et al. [12] indicated that the multi-objective grey wolf method is superior to the non-dominated genetic and particle swarm optimization algorithms. The algorithm's results are divided into three groups: alpha (α), beta (β), and delta (δ) wolves, with alpha wolves being the best. These wolves generate the Pareto frontier of the optimal solution points as they mimic and lead the optimization issue toward convergence. The optimization algorithm should first create and apply the following terms to describe the surrounding behavior of grey wolves:

$$\vec{D} = \left| \vec{C}.\vec{X}_P(t) - \vec{X}(t) \right| \tag{21}$$

$$\vec{X}(t+1) = \vec{X}_P(t) - \vec{A}.\vec{D} \tag{22}$$

$$\vec{A} = 2\vec{a}.\vec{r}_1 - \vec{a} \tag{23}$$

$$\vec{C} = 2.\vec{r}_2 \tag{24}$$

The current iteration is represented by t. The prey position vector is denoted by $\vec{X}_P$ while the single wolf position vector is denoted by $\vec{X}$. Moreover, $\vec{A}$ and $\vec{C}$ denote the coefficient-related vectors as follow:

Table 4
The equipment's purchased cost to calculate the operating/maintenance/investment formulas [43–46].

Equipment	Z_k ($)
Electrolyzer	$Z_{Electrolyzer} = c_1 \times \dot{W}_{Electrolyzer}$ $c_1 = 1246\ \$/kWh$
Fuel cell	$Z_{Fuel\ cell} = c_2 \times \dot{W}_{Fuel\ cell}$ $c_2 = 3115\ \$/kWh$
VCl cycle	$Z_{VCl} = c_3 \times \dot{m}_{Hydrogen} \times LHV_{Hydrogen}$ $c_3 = 0.125\ \$/kW$
Trough collectors	$Z_{Collectors} = c_4 \times A_{Total}$ $c_4 = 240\ \$/m^2$
Wind turbine	$Z_{Turbine} = c_5 \times N_{Turbine}$ $c_5 = 8163\ \$/Number$
Hydrogen tank	$Z_{Hydrogen\ tank} = c_6 \times V_{Hydrogen\ tank}$ $c_6 = 245\ \$/m^3$
Hot water tank	$Z_{Water\ tank} = c_7 \times V_{Water\ tank}$ $c_7 = 7872\ \$/m^3$
Absorption chiller	$Z_{Chiller} = c_8 \times \dot{Q}_{Cooling}$ $c_8 = 707\ \$/kWh$
Heat exchanger	$Z_{Heat\ exchanger} = c_9 \times A^{0.6}_{Heat\ exchanger}$ $c_9 = 750\ \$/m^{1.2}$
Pump	$Z_{Pump} = c_{10} \times \dot{W}^{0.71}_{Pump}$ $c_{10} = 3540\ \$/kWh^{0.71}$
Valve	$Z_{Valve} = 140\ \$/unit$
Controller	$Z_{Controller} = 276.6\ \$/unit$

$i = 10\ \%$, $\tau = 20$, and $n = 7446$.

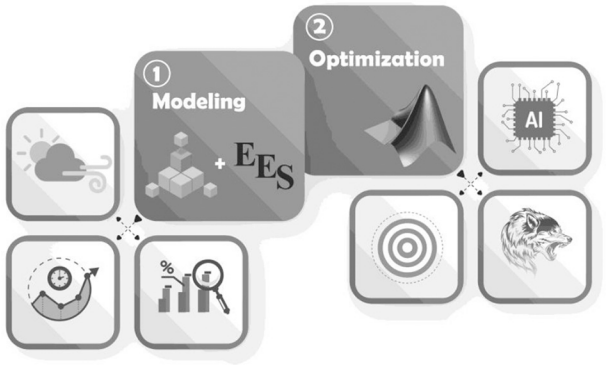

Fig. 7. The optimization procedure applied to the proposed smart system.

$$\vec{A} = 2\vec{a}.\vec{r}_1 - \vec{a} \tag{25}$$

$$\vec{C} = 2.\vec{r}_2 \tag{26}$$

in which r_1 and r_2 are random vectors between zero and one. The MOGWO only considers the first three best solutions. Search agents are also required to adjust their positions following previously stated solutions by this algorithm. The following equations must be used in the algorithm to keep track of the position:

$$\vec{D}_i = \left|\vec{C}_m.\vec{X}_i - \vec{X}\right| \tag{27}$$

$$\vec{X}_m = \vec{X}_i - \vec{A}_m.\left(\vec{D}_i\right) \tag{28}$$

$$\vec{X}(t+1) = \frac{\vec{X}_1 + \vec{X}_2 + \vec{X}_3}{3} \tag{29}$$

i could be alpha, beta, or delta, while m is 1, 2, or 3 for the alpha, beta, and delta wolves. Further details on grey wolf optimization can be found in Reference [50]. Finally, decisions are made using various criteria to find the best optimization point, which simultaneously meets conflicting objectives. In the present study, the TOPSIS technique as a multi-criteria decision-making method is used to finalize the optimization results. Yoon and Hwang [51] pioneered the use of the TOPSIS (Technique for Order Preference Similarity to Ideal Solution) method. The process of TOPSIS implementation consists of seven steps. First, a decision matrix for the ranking should be established. Then, the decision matrix is normalized as follows:

$$r_{ij} = x_{ij}\sqrt{\sum_{i-1}^{m} x_{ij}^2}\ i = 1,2,\ldots,\mathrm{m} \text{ and } \mathrm{j} = 1,2,\ldots,\mathrm{n} \tag{30}$$

Third, the weighted normalized value of the decision matrix is evaluated as shown by Eq. (31):

$$v_{ij} = r_{ij} \times W_j\ \mathrm{i} = 1,2,\ldots,\mathrm{m} \text{ and } \mathrm{j} = 1,2,\ldots,\mathrm{n} \tag{31}$$

In this equation, W_j denotes the weight of the j^{th} criterion. Afterward, the ideal and negative ideal solutions are determined as below, respectively:

$$A^* = \left\{\left(maxv_{ij} \mid \mathrm{j} \in C_b\right), \left(minv_{ij} \mid \mathrm{j} \in C_C\right)\right\} = \left\{v_j^* \mid \mathrm{j} = 1,2,\ldots,\mathrm{m}\right\} \tag{32}$$

$$A^- = \left\{\left(maxv_{ij} \mid \mathrm{j} \in C_b\right), \left(minv_{ij} \mid \mathrm{j} \in C_C\right)\right\} = \left\{v_j^- \mid \mathrm{j} = 1,2,\ldots,\mathrm{m}\right\} \tag{33}$$

Subsequently, the m-dimensional Euclidean distance should be used to compute the distances. The following criteria assess each option's distance from the positive and negative ideal solutions:

$$S_i^* = \sqrt{\sum_{j=1}^{m}\left(v_{ij} - v_j^*\right)^2}\ \mathrm{j} = 1,2,\ldots,\mathrm{m} \tag{34}$$

$$S_i^- = \sqrt{\sum_{j=1}^{m}\left(v_{ij} - v_j^-\right)^2}\ \mathrm{j} = 1,2,\ldots,\mathrm{m} \tag{35}$$

Afterward, the relative closeness to the ideal solution is evaluated as follows:

$$RC_i^* = \frac{S_i^-}{S_i^* + S_i^-}\ \mathrm{i} = 1,2,\ldots,\mathrm{m} \tag{36}$$

Eventually, the preference order will be ranked to determine the best optimization answer.

3. Results and discussion

TRNSYS software, which is distinguished by a wide library of components for transient modeling of smart energy systems, is used to study the system's performance from thermodynamic, economic, and environmental points of view. In addition, a parametric analysis is carried out to investigate the impact of major design variables on key metrics from different aspects. Afterward, the grey wolf approach is used to apply four-objective optimization to the proposed system in order to increase primary energy saving and carbon dioxide emission reduction rates and simultaneously decrease cost rate and energy bought from the network. Besides, the scatter distribution of major design variables is shown to better represent the system's behavior at the optimal condition. Finally, the hourly, monthly, and annual variations of significant performance indicators from various perspectives are analyzed for the optimal operating condition achieved by the grey wolf algorithm.

3.1. Parametric results

Since the collector's physical appearances play a significant part in the solar system's efficiency, Fig. 8 indicates the impact of collector length on bought energy, total cost rate, and primary energy saving and carbon dioxide reduction rate.

The higher collector length results in more received solar radiation and, thereby a higher produced hydrogen by the thermochemical cycle. Therefore, the dependence on solar energy to fill the hydrogen tank rises, and the electrolyzer electricity use will decrease. Fig. 8 shows that the PESR and CDERR will increase about 17 % and 25 %, respectively, when the collector length increases from 30 m to 45 m. This is reasonable because higher electricity is sold to the local network by decreasing the electrolyzer required energy (take a look at Eq. (12) and Eq. (18)). Fig. 8 further demonstrates that as the size of the collector gets larger, the total cost also increases by about 4 $/h, which is not ideal from an economic standpoint. This makes sense, given that the cost of purchasing a collector rises in proportion to the area it covers. Eventually, from Fig. 8, it can be concluded that by increasing the collector length, the energy bought from the local electricity and heating networks over a year increases slightly (about 100 kWh), which is negligible. The importance of four-objective optimization, which identifies the ideal operating condition where all objectives are met, is revealed by the simultaneous increase in favorable (PESR and CDERR) and unfavorable (total cost rate and bought energy) indicators.

In Fig. 9, the variation of bought energy from the networks, primary energy saving and carbon dioxide reduction rates, and total cost rate with electrolyzer electrode area is demonstrated. Fig. 9 reveals that the amount of energy bought from networks increases by about 150 kWh if the area rises from 0.1 m^2 to 0.25 m^2. This is justified because a bigger

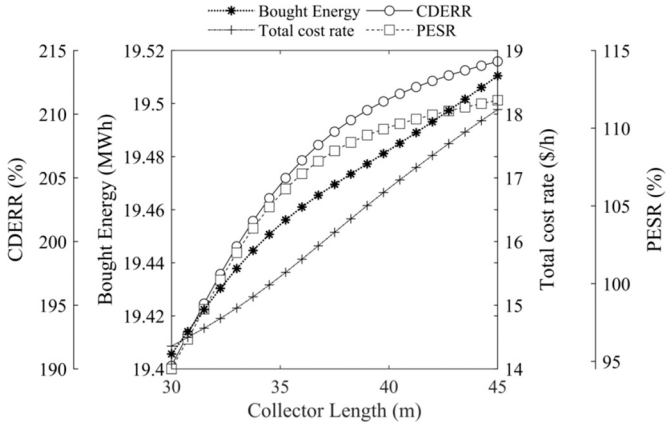

Fig. 8. The impact of collector length on techno-economic-environmental metrics.

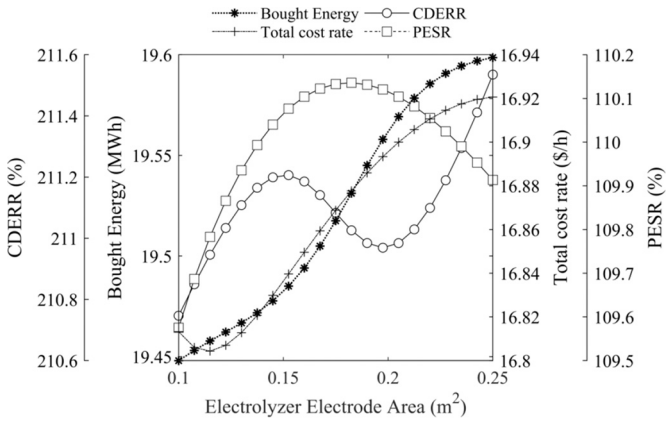

Fig. 9. The impact of electrolyzer electrode area on techno-economic-environmental metrics.

electrode requires higher input electricity to split the water into hydrogen and oxygen. Therefore, extra required electricity must be supplied from the electricity grid (not the wind turbine) since the rest components' size, including the wind turbine, is fixed. According to the figure, when the electrode area increases from 0.1 m^2 to 0.25 m^2, PESR increases to a certain value and then falls. The figure further depicts that the CDERR is highly sensitive to electrode area. In this regard, by growing the electrode area from 0.1 m^2 to 0.25 m^2, the CDERR increases 0.5 %, then decreases by 0.25 %, and finally rises to 211.5 %. What stands out from Fig. 9 is that since CDERR and PESR vary by <1 %, it may be concluded that the electrode area does not affect these parameters. The figure finally presents that picking up a higher electrode area is not economically favorable due to the increment in the total cost rate. This is rational because the electrolyzer investment cost is directly proportional to the electricity use.

Fig. 10 illustrates the variation of the proposed smart building energy system indicators from the techno-economic and environmental aspects with the hydrogen tank volume. The more hydrogen tank capacity leads to a lower electrolyzer power use, so more electricity generated by the wind turbine could be sold to the local grid. According to Fig. 10, the increase in hydrogen tank volume is techno-environmentally desirable because higher PESR and CDERR are achieved. The total cost rate, on the other hand, rises as the hydrogen tank's purchasing cost rises with the tank's capacity. As depicted, the total cost rate rises by about 0.2 $/h by increasing the tank volume from 40 m^3 to 70 m^3. Furthermore, it can be obtained that the system's dependence on renewable resources will increase because the bought energy is reduced by rising the tank volume. Furthermore, Fig. 10 demonstrates that the system's reliance on renewable resources would increase because the bought energy is reduced by increasing the tank volume. The conflicting variance between the targets reveals the necessity of multi-objective optimization, such as increasing the total cost rate while lowering bought energy.

The influence of fuel cell current on the proposed smart system is investigated and presented in Fig. 11. As shown, the current has a significant impact on techno-environmental metrics. Higher hydrogen is consumed in the fuel cell by increasing the current from 300 A to 500 A. Therefore, a higher power is generated, and considerable electricity and heating could be sold to the local energy networks. According to Fig. 11, the increment of current leads to around a 50 % increase in PESR, which is significant. In addition, Fig. 11 exhibits that the majority of energy cost paid by the owner could be mitigated since the annual energy bought from local networks decreases by about 5MWh by picking up the fuel cell current. The figure further demonstrates that bringing the current up from 300 A to 420 A will increase the total cost rate. According to Table 4, this assertion is plausible because the formula for the purchasing cost of the fuel cell is proportionate to the power it generates. Subsequently, Fig. 11 shows that the total cost rate falls about 0.15 $/h when the current increases from 420 A to 500 A. This is defendable because the investment cost decrement of other components due to decreased size/energy is higher than the purchased cost increment of the fuel cell. Eventually, Fig. 11 indicates that when the current increases, the CDERR rises dramatically and subsequently decreases slightly.

Fig. 12 shows the impact of fuel cell voltage, a crucial parameter that highly affects the fuel cell and the entire system performance from techno-economic and environmental points of view. A higher cell voltage leads to a higher power generated by the Alkaline fuel cell stack; ergo, the net electricity sold to the local grid will increase. Conversely, lower waste heat could be recovered from the fuel cell by increasing the cell voltage. Therefore, the net produced heating will decrease, and higher energy must be bought from the district heating network to supply the building's load, as shown in Fig. 12. Moreover, the figure depicts that considerably higher PESR and CDERR of 65 % and 150 %, respectively, are achieved by increasing the cell voltage from 3.5 V to 7.5 V because the increase in energy electricity sold to the local grid is higher than the increment of heat purchased from the district heating network. The rise in cell voltage is economically undesirable because of the fuel cell unitless investment cost growth, which is a function of the electricity production, as displayed in Fig. 12. According to the figure, as the cell voltage increases from 3.5 V to 7.5 V, the total cost rate increases from 16 $/h to 18.25 $/h.

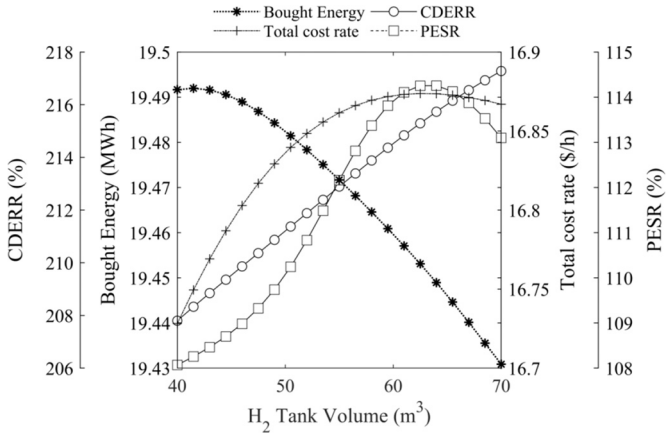

Fig. 10. The impact of hydrogen tank volume on techno-economic-environmental metrics.

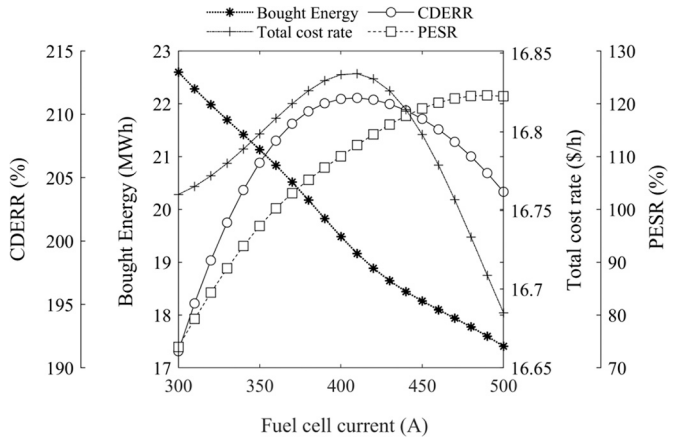

Fig. 11. The impact of fuel cell current on techno-economic-environmental metrics.

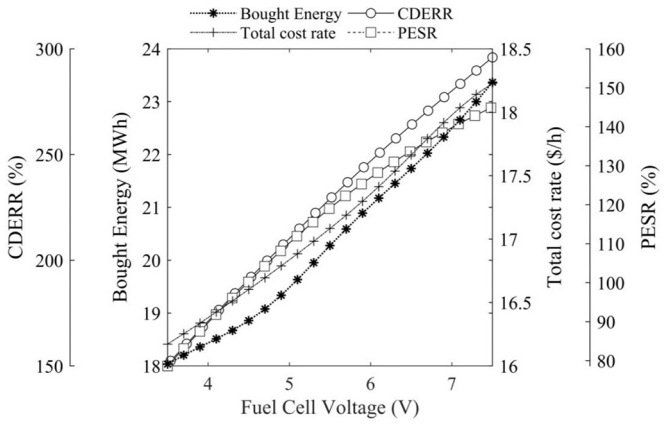

Fig. 12. The impact of fuel cell voltage on techno-economic-environmental metrics.

3.2. Optimization results

Following a thorough parametric analysis, the four-objective grey wolf optimization method is used in MATLAB to test the effectiveness of the proposed technique and identify the best possible solution points from various perspectives. Fig. 13 demonstrates the four-dimensional Pareto frontier diagram of techno-economic-environmental objectives comprising the total cost rate, bought energy, and primary energy saving and carbon dioxide emission reduction rates. As indicated, many conflicting optimum points can be found in the Pareto diagram, graded according to the strategies of the decision-makers. While the bought energy and total cost rate reach the maximum values of 15.5 MWh and 13.6 $/h at Point A, the highest PESR and CDERR of 81.3 % and 238.5 % corresponds to Point B. According to Fig. 13, it is impossible to spot an optimal position with the greatest PESR and CDERR and the least total cost rate and energy bought from the local networks due to the conflicting values of objective functions. Hence, the optimum locations are ranked using the TOPSIS approach, a multi-criteria decision-making method, regarding their distance from the ideal and negative-ideal solutions. Using this method, the best optimization point is the TOPSIS point (see Fig. 13), which simultaneously meets four conflicting objectives.

Table 5 provides specific information regarding the values of the objective functions, the most important design parameters, and other performance indicators at Points A, B, and TOPSIS. According to the table, at the TOPSIS point, the optimum value of the total cost rate, bought energy, and primary energy saving and carbon dioxide emission reduction rates are 14.8 $/h, 24.9 MWh, 80.6 %, and 219 %. This condition is achieved by choosing the fuel cell current, electrode area, H_2 tank volume, collector length, and fuel cell voltage of 303.3 A, 0.17 m^2, 49.7 m^3, 30.2 m, and 6.4 V, respectively. However, the optimization results are constrained by several factors that make improving primary energy and CO_2 savings difficult even when the cost rate and bought energy are brought down to the optimized levels. The first limitation is the amount of sunlight availability, in addition to the high rate of heat loss and low energy conversion rate that occurs within the solar system. The next limitation includes the decision parameters range that has a maximum allowable increase or decrease and is therefore fixed at a specific domain.

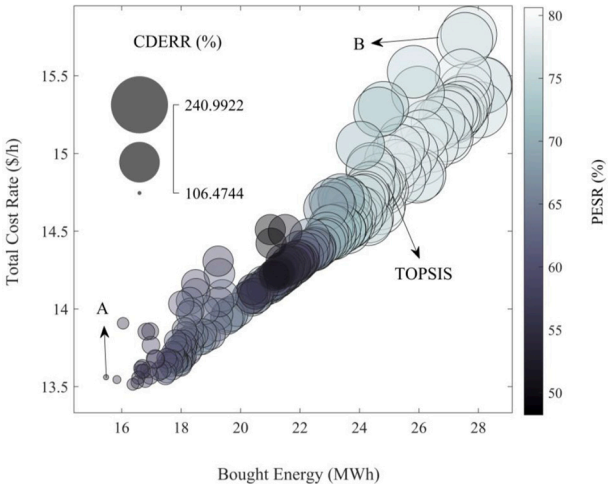

Fig. 13. Four-dimensional Pareto frontier diagram of the total cost rate, bought energy, and primary energy saving and carbon dioxide emission reduction rates.

Table 5
Detailed optimization outcomes extracted from the Pareto frontier diagram at Pint A, Point B, and TOPSIS.

	Parameter	Point A	Point B	TOPSIS
Components' best size	Fuel cell current (A)	500	300	303.3
	Electrolyzer electrode area (m^2)	0.16	0.1	0.17
	H_2 tank volume (m^3)	43.5	70	49.7
	Collector length (m)	30	30	30.2
	Fuel cell voltage (V)	3.5	7.4	6.4
Objective functions	Total cost rate ($/h)	13.6	15.8	14.8
	CDERR (%)	107	238.4	219
	PESR (%)	56	81.3	80.6
	Bought energy (MWh)	15.5	27.7	24.9
Other performance indicators	Hydrogen produced by electrolyzer (m^3/h)	3755.8	1703.5	1663.2
	Hydrogen produced by VCl cycle (m^3/h)	19,671.6	19,671.6	19,796.2
	Power generated by fuel cell (MWh)	1.8	40.6	32.9
	Power generated by wind turbine (MWh)	17.5	17.5	17.5
	Cooling generated by chiller (MWh)	9.8	9.8	9.8
	Total heat generation (MWh)	57.3	25.6	32.3
	ACSR (%)	108.2	164.7	160.8

In order to get a better insight into the distribution of optimum points across the population size, the histogram diagram is illustrated in Fig. 14. Fig. 14(a) demonstrates that the fuel cell current should be kept below 320 A to achieve the optimal techno-economic-environmental condition. What stands out from Fig. 14(b) is that the electrode area is insensitive since its optimal points are scattered throughout the whole domain. According to s 14(c) and 14(d), H_2 tank volume and collector length are effective variables, and their change will substantially impact the performance metrics because the bulk of optimal points is close to the lowest range. Eventually, Fig. 14(e) shows that the fuel cell voltage optimum points are scattered between 3.5 V and 5 V, most of which are close to the lower limit.

3.3. Transient results

After the parametric study and four-objective optimization, hourly, monthly, and seasonal variations of significant performance indicators under optimal conditions are investigated in the following figures. As mentioned above, two-way interaction with the local energy networks through a rule-based controller strategy is one of the most important aspects of the proposed smart building system. For this, the hourly variation and time duration curve of the net energy sold/bought to/from the electricity and district heating networks are demonstrated in Fig. 15. According to the figure, most of the time (70 % of the year), the net energy is positive, which means that the proposed renewable-driven

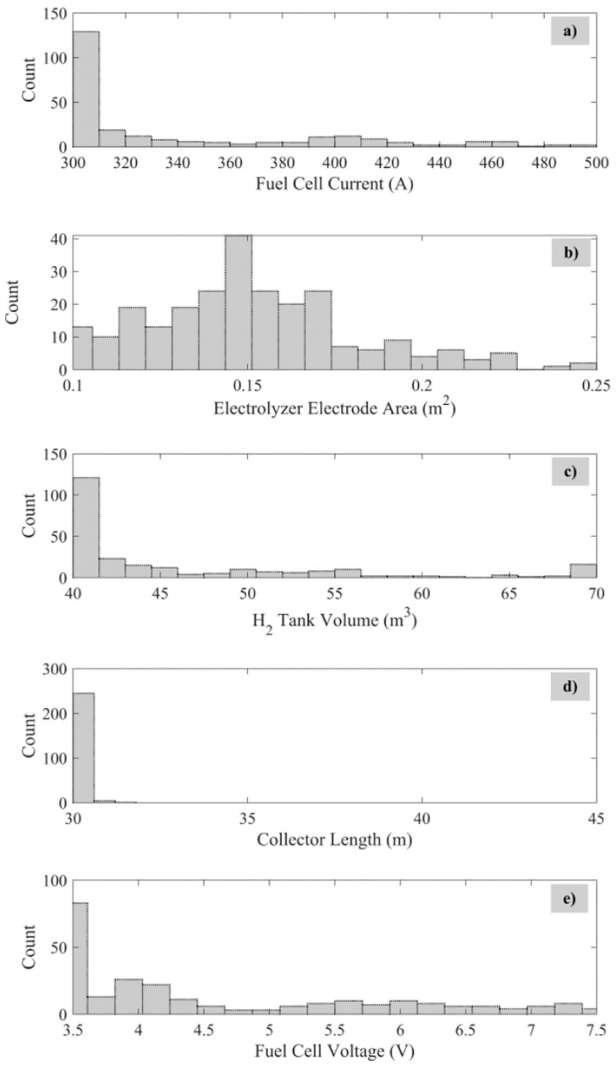

Fig. 14. The histogram diagram of the main operational parameters.

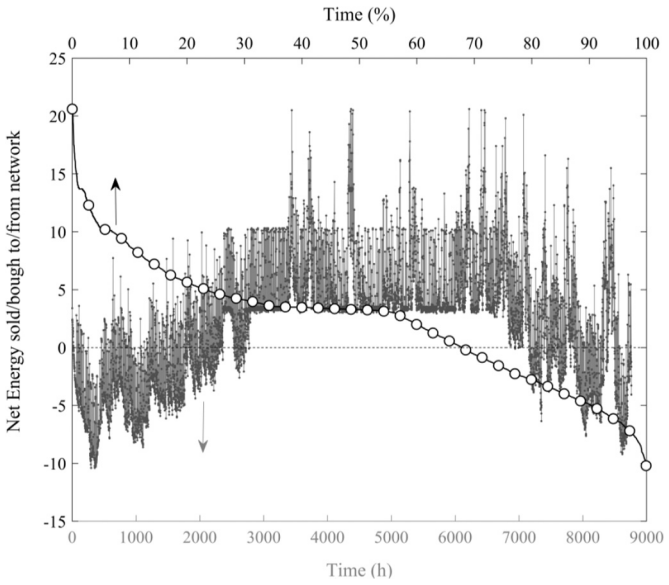

Fig. 15. The hourly variation and time duration curve of net energy sold/bought to/from the networks.

smart system can autonomously supply the building's demand and sell the surplus production to the local network. The figure further depicts that while the maximum energy bought from the networks in the absence of solar and wind resources is 10.37 kWh, the highest value of energy sold reaches up to 20.55 kWh, which is considerable.

Furthermore, it can be observed that the proposed system can sell at least 3.7 kWh electricity and heating to the local networks for >55 % of the year, revealing the significance of the proposed intelligent strategy to compensate for the building's energy bill. From the hourly variation, it can be concluded that the building's dependence on the local energy networks is higher in the cold hours since there is a lack of solar availability to run the smart system. Consequently, the net energy is below the x-axis in most of winter and autumn, as indicated in Fig. 15.

In order to have a better overview of the effect of solar and wind availability on the proposed system's performance, Fig. 16 presents the variation of average hourly net energy sold/bought to/from the networks over each month. According to the figure, the system must be wholly supplied by the local electricity and district heating networks because the average hourly energy is always negative in January and February. The figure further shows that the average hourly values are positive from April to October because abundant available solar and wind resources generate hydrogen for storage in the tank. Therefore, the proposed building energy system could not only operate off-grid but also sell the extra generation to the networks. According to the figure, the highest average hourly sold and bought energies are 9.139 kWh and − 5.465 kWh at 6:00 and 22:00 in July and January, respectively.

Fig. 17 presents the monthly variation of hydrogen produced by the electrolyzer and VCl cycle to reflect the contribution of solar and wind resources in providing the building's energy demand over the year. According to the figure, increasing the temperature and radiation from January to June increases the share of solar energy, and higher hydrogen is generated through the VCl cycle. From the figure, it can also be concluded that, in warm months, a higher power generated by a wind turbine is sold to the electricity grid since the solar energy can supply the H_2 tank standalone. In contrast, the figure reveals that in cold months the share of wind energy in hydrogen storage is considerably higher than the solar resource. It demonstrates the importance of hybridizing two different renewable resources to obtain a building energy system with the lowest dependent on local energy networks. According to Fig. 17, the contribution of wind energy to hydrogen production is >75 %, 45 %, and 25 % in January, February, and March, respectively.

Fig. 18 indicates the monthly and seasonal power and heating generation via renewable resources for the proposed building energy system in Lund, Sweden. According to the figure, the highest monthly heating and power production of 19 MWh alludes to August. The figure further shows that the minimum monthly heating and power generation of 2.6 MWh are attained in January. Moreover, Fig. 18 reveals that while the highest total renewable energy of 48.7 MWh is produced during the summer, the minimum seasonal generation corresponds to winter with the value of 8.6 MWh.

As previously noted, compared to conventional systems, environmental friendliness is one of the superiority of the proposed smart building system because it does not use fossil fuels for power, heating, and cooling needs. Fig. 19 illustrates the techno-economic-environmental benefits of the proposed smart system considering a neighborhood with 100 building complexes in Lund. According to Fig. 19, the suggested smart system has several environmental advantages. In Sweden, for every MWh of electricity and heating produced, CO_2 emissions of 8 kg and 5.09 kg are generated in the traditional system [49]. Therefore, using the suggested smart system for the Lund case study can minimize 13,920 kg and 47,838 kg of CO_2 emissions for electricity and heating generation based on an annual total electricity and heating production of 1740 MWh and 9380 MWh, respectively. Moreover, it is estimated that each kilogram of CO_2 emissions costs 0.125 dollars to the environment, considering Sweden [52]. In other words, establishing the proposed system saves the environment 7719

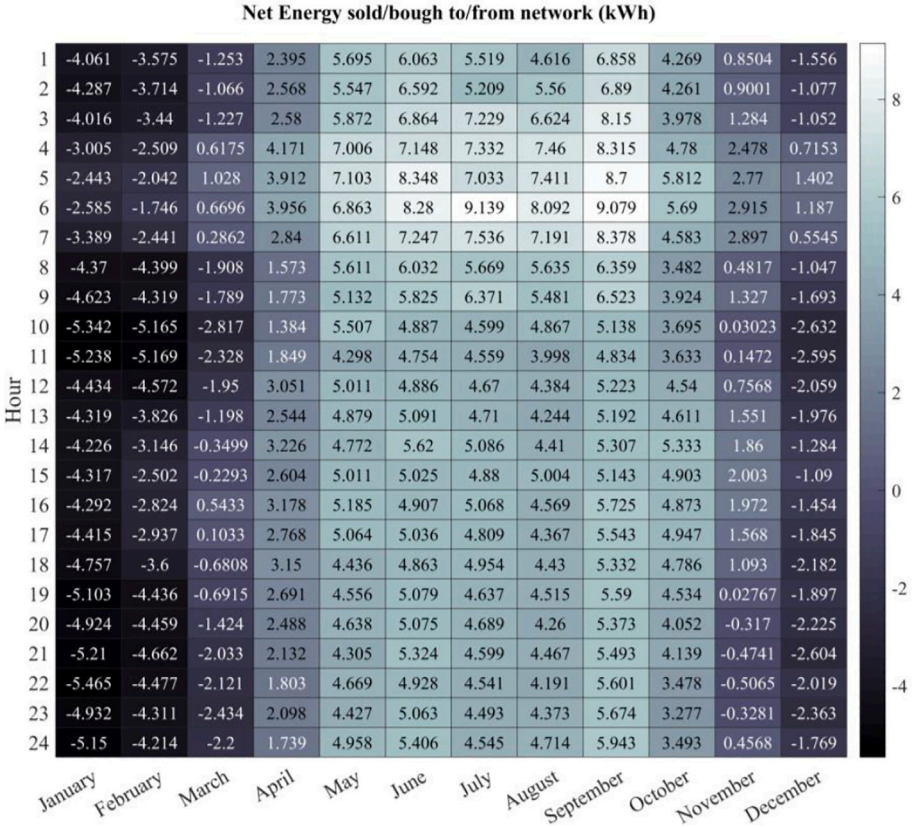

Fig. 16. The monthly variation of net energy sold/bought to/from the networks.

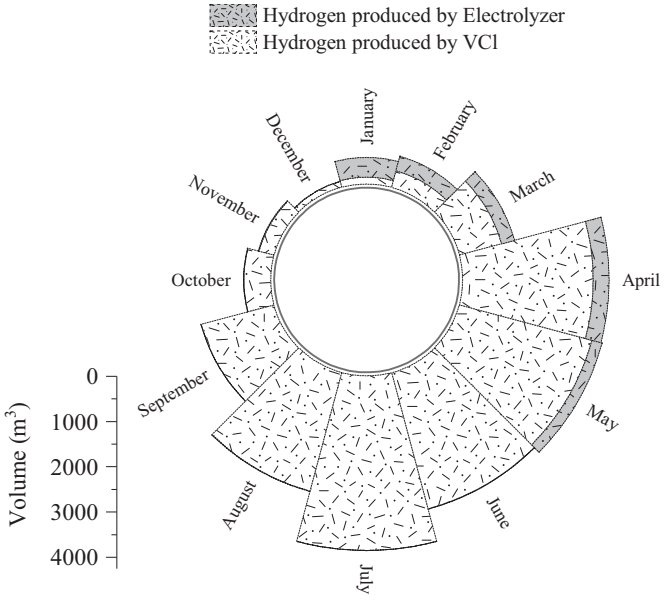

Fig. 17. The monthly variation of hydrogen produced by the electrolyzer and VCl cycle.

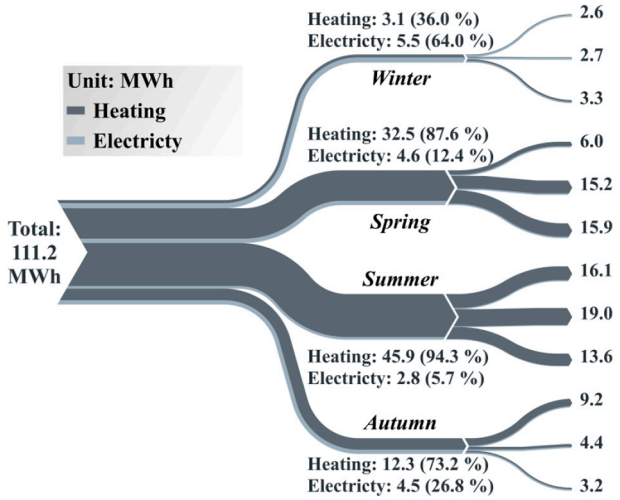

Fig. 18. Monthly and seasonal variations of heating and electricity produced by renewable resources.

dollars a year for electricity and heating production, equivalent to adding 6.9 ha of new green space and plants, as depicted in Fig. 19.

4. Conclusion

This paper present and thoroughly investigates an innovative, clean, and effective smart hydrogen production/storage system driven by solar and wind resources for shaving the peak load and stabilizing the grid. A rule-based control method is created to establish an intelligent two-way interaction with district heating and electricity networks to offset the yearly energy costs and motivate householders to move toward their own renewable-based energy plant. Moreover, as a passive performance enhancement approach, the low-temperature waste heat is recovered from the Alkaline fuel cells to provide the heating and cooling demands. The practicality of the suggested system is evaluated for a multi-family building complex in Lund, Sweden, from techno-economic and environmental points of view. Transient simulation is performed through TRNSYS and the engineering equation solver program to calculate the

Fig. 19. Techno-economic-environmental benefits of the proposed smart system for a neighborhood with 100 building complexes.

most significant performance indicators and compare them with the existing system. Subsequently, the smart system is optimized via an artificial neural network combined with the grey wolf algorithm in MATLAB software to mitigate the system's cost while improving the techno-environmental conditions simultaneously. The main outcomes could be outlined as follows:

- The simultaneous increase in desirable (primary energy saving and carbon dioxide emission reduction rate) and unfavorable (total cost rate and bought energy) indicators highlights the significance of four-objective optimization to meet more than three conflictive metrics.
- The optimal values for primary energy saving, carbon dioxide emission reduction rate, total cost rate, and the bought energy at the four-objective optimization point using the grey wolf optimizer are 80.6 %, 219 %, 14.8 $/h, and 24.9 MWh, respectively.
- What stands out from the scatter distribution of main design parameters the electrode area is insensitive because its ideal points are dispersed throughout the entire domain. However, it is recommended to maintain the H_2 tank volume and collector length at their minimum levels.
- Thanks to the two-way interaction with the local energy networks via a rule-based control strategy, the suggested renewable-driven smart system can autonomously supply the building's needs and sell the excess production to the local network at 70 % of the year.
- In the winter, wind energy constitutes a far larger portion of hydrogen storage than solar energy, highlighting the benefits of integrating different renewable energy sources to create a building energy system that is least reliant on regional energy grids.
- The proposed renewable-based smart system can reduce CO_2 emissions by 13,920 kg for electricity generation and 47,838 kg for heating generation, resulting in a reduction of 7719 dollars in environmental costs, equivalent to 6.9 ha of reforestation in Lund.

Eventually, a couple of recommendations for continuing or improvement of the current research could be suggested as follows:

- Performing exergy/exergoeconomic assessment to analyze and compare the proposed smart system from the irreversibility aspect.
- Comparing the techno-economic-environmental indicators of the proposed model with the same system equipped with photovoltaic panels instead of the wind turbine.
- Establishing advanced control approaches like model predictive control to more effectively monitor and manage the energy production/usage/storage and different operation modes.

CRediT authorship contribution statement

Amirmohammad Behzadi: Investigation, Methodology, Software, Validation, Writing – original draft. **Seyed Mojtaba Alirahmi:** Visualization, Software, Methodology. **Haoshui Yu:** Writing – review & editing, Supervision, Data curation. **Sasan Sadrizadeh:** Writing – review & editing, Supervision, Data curation, Funding acquisition.

Declaration of competing interest

The authors declare that they have no known competing financial interests or personal relationships that could have appeared to influence the work reported in this paper.

Data availability

Data will be made available on request.

Acknowledgment

The authors are grateful to the Swedish Energy Agency (Energimyndigheten) for partly financing this research study. This article is drafted in line with Annex 37 (Smart Design and Control of Energy Storage Systems).

References

[1] M. Gutsch, J. Leker, Global warming potential of lithium-ion battery energy storage systems: a review, J. Energy Storage 52 (2022), 105030, https://doi.org/10.1016/j.est.2022.105030.
[2] S.B. Sani, P. Celvakumaran, V.K. Ramachandaramurthy, S. Walker, B. Alrazi, Y. J. Ying, N.Y. Dahlan, M.H.A. Rahman, Energy storage system policies: way forward and opportunities for emerging economies, J. Energy Storage 32 (2020), 101902, https://doi.org/10.1016/j.est.2020.101902.
[3] A. Behzadi, S. Holmberg, C. Duwig, F. Haghighat, R. Ooka, S. Sadrizadeh, Smart design and control of thermal energy storage in low-temperature heating and high-temperature cooling systems: a comprehensive review, Renew. Sust. Energ. Rev. 166 (2022), 112625, https://doi.org/10.1016/j.rser.2022.112625.
[4] S. Jafari, M. Ameri, Integrating photovoltaic/linear fresnel reflector with supercritical carbon dioxide energy storage system: energy and exergy analysis, J. Energy Storage 53 (2022), 105235, https://doi.org/10.1016/j.est.2022.105235.
[5] N. Soni, D. Sharma, M.M. Rahman, P.R. Hanmaiahgari, V.M. Reddy, Mathematical modeling of solar energy based thermal energy storage for house heating in winter, J. Energy Storage 34 (2021), 102203, https://doi.org/10.1016/j.est.2020.102203.
[6] T.K. Aseri, C. Sharma, T.C. Kandpal, A techno-economic appraisal of parabolic trough collector and central tower receiver based solar thermal power plants in India: effect of nominal capacity and hours of thermal energy storage, J. Energy Storage 48 (2022), 103976, https://doi.org/10.1016/j.est.2022.103976.
[7] N. Bechir, R. Chargui, B. Tashtoush, M. Lazaar, Performance analysis of a novel combined parabolic trough collector with ejector cooling system and thermoelectric generators, J. Energy Storage 47 (2022), 103584, https://doi.org/10.1016/j.est.2021.103584.
[8] Q. Wang, G. Pei, H. Yang, Techno-economic assessment of performance-enhanced parabolic trough receiver in concentrated solar power plants, Renew. Energy 167 (2021) 629–643, https://doi.org/10.1016/j.renene.2020.11.132.
[9] G. Kumaresan, R. Sridhar, R. Velraj, Performance studies of a solar parabolic trough collector with a thermal energy storage system, Energy 47 (2012) 395–402, https://doi.org/10.1016/j.energy.2012.09.036.
[10] Q. Wu, C. Li, Economy-environment-energy benefit analysis for green hydrogen based integrated energy system operation under carbon trading with a robust optimization model, J. Energy Storage 55 (2022), 105560, https://doi.org/10.1016/j.est.2022.105560.
[11] P. Marocco, D. Ferrero, A. Lanzini, M. Santarelli, The role of hydrogen in the optimal design of off-grid hybrid renewable energy systems, J. Energy Storage 46 (2022), 103893, https://doi.org/10.1016/j.est.2021.103893.
[12] A. Behzadi, E. Gholamian, S.M. Alirahmi, B. Nourozi, S. Sadrizadeh, A comparative evaluation of alternative optimization strategies for a novel heliostat-driven hydrogen production/injection system coupled with a vanadium chlorine cycle, Energy Convers. Manag. 267 (2022), 115878, https://doi.org/10.1016/j.enconman.2022.115878.
[13] M. Ouagued, A. Khellaf, L. Loukarfi, Performance analyses of Cu–Cl hydrogen production integrated solar parabolic trough collector system under algerian climate, Int. J. Hydrog. Energy 43 (2018) 3451–3465, https://doi.org/10.1016/j.ijhydene.2017.11.040.
[14] F. Yilmaz, R. Selbaş, Thermodynamic performance assessment of solar based sulfur-iodine thermochemical cycle for hydrogen generation, Energy 140 (2017) 520–529, https://doi.org/10.1016/j.energy.2017.08.121.

[15] M.T. Balta, I. Dincer, A. Hepbasli, Performance assessment of solar-driven integrated mg-cl cycle for hydrogen production, Int. J. Hydrog. Energy 39 (2014) 20652–20661, https://doi.org/10.1016/j.ijhydene.2014.06.133.
[16] M. Temiz, I. Dincer, Concentrated solar driven thermochemical hydrogen production plant with thermal energy storage and geothermal systems, Energy 219 (2021), 119554, https://doi.org/10.1016/j.energy.2020.119554.
[17] M.T. Balta, I. Dincer, A. Hepbasli, Comparative assessment of various chlorine family thermochemical cycles for hydrogen production, Int. J. Hydrog. Energy 41 (2016) 7802–7813, https://doi.org/10.1016/j.ijhydene.2015.12.222.
[18] A. Behzadi, A. Arabkoohsar, M. Sadi, K.H. Chakravarty, A novel hybrid solar-biomass design for green off-grid cold production, techno-economic analysis and optimization, Sol. Energy 218 (2021) 639–651, https://doi.org/10.1016/j.solener.2021.02.065.
[19] T. Yi, H. Ye, Q. Li, C. Zhang, W. Ren, Z. Tao, Energy storage capacity optimization of wind-energy storage hybrid power plant based on dynamic control strategy, J. Energy Storage 55 (2022), 105372, https://doi.org/10.1016/j.est.2022.105372.
[20] H. Ishaq, I. Dincer, G.F. Naterer, Development and assessment of a solar, wind and hydrogen hybrid trigeneration system, Int. J. Hydrog. Energy 43 (2018) 23148–23160, https://doi.org/10.1016/j.ijhydene.2018.10.172.
[21] M.M. Hasan, G. Genç, Techno-economic analysis of solar/wind power based hydrogen production, Fuel 324 (2022), 124564, https://doi.org/10.1016/j.fuel.2022.124564.
[22] B. Wang, X. Yu, J. Chang, R. Huang, Z. Li, H. Wang, Techno-economic analysis and optimization of a novel hybrid solar-wind-bioethanol hydrogen production system via membrane reactor, Energy Convers. Manag. 252 (2022), 115088, https://doi.org/10.1016/j.enconman.2021.115088.
[23] A.S. Al-Buraiki, A. Al-Sharafi, Hydrogen production via using excess electric energy of an off-grid hybrid solar/wind system based on a novel performance indicator, Energy Convers. Manag. 254 (2022), 115270, https://doi.org/10.1016/j.enconman.2022.115270.
[24] Z. Wang, X. Zhang, A. Rezazadeh, Hydrogen fuel and electricity generation from a new hybrid energy system based on wind and solar energies and alkaline fuel cell, Energy Rep. 7 (2021) 2594–2604, https://doi.org/10.1016/j.egyr.2021.04.060.
[25] Y. Guo, A. Yousefi, Determining the appropriate size of the electrical energy storage system of an energy process based on a solid oxide fuel cell and wind turbine, J. Energy Storage 44 (2021), 103430, https://doi.org/10.1016/j.est.2021.103430.
[26] D. Li, J. Guo, J. Zhang, L. Zhan, M. Alizadeh, Numerical assessment of a hybrid energy generation process and energy storage system based on alkaline fuel cell, solar energy and Stirling engine, J. Energy Storage 39 (2021), 102631, https://doi.org/10.1016/j.est.2021.102631.
[27] D. Wei, L. Zhang, A.A. Alotaibi, J. Fang, A.H. Alshahri, K.H. Almitani, Transient simulation and comparative assessment of a hydrogen production and storage system with solar and wind energy using TRNSYS, Int. J. Hydrog. Energy (2022), https://doi.org/10.1016/j.ijhydene.2022.02.157.
[28] S. Wang, W. Li, H. Fooladi, Performance evaluation of a polygeneration system based on fuel cell technology and solar photovoltaic and use of waste heat, Sustain. Cities Soc. 72 (2021), 103055, https://doi.org/10.1016/j.scs.2021.103055.
[29] Y. Shen, X. Li, N. Wang, L. Li, A. Hoseyni, Introducing and investigation of a pumped hydro-compressed air storage based on wind turbine and alkaline fuel cell and electrolyzer, Sustain. Energy Technol. Assess. 47 (2021), 101378, https://doi.org/10.1016/j.seta.2021.101378.
[30] P. Pal, V. Mukherjee, Off-grid solar photovoltaic/hydrogen fuel cell system for renewable energy generation: an investigation based on techno-economic feasibility assessment for the application of end-user load demand in north-east India, Renew. Sust. Energ. Rev. 149 (2021), 111421, https://doi.org/10.1016/j.rser.2021.111421.
[31] S.M. Alirahmi, A. Khoshnevisan, P. Shirazi, P. Ahmadi, D. Kari, Soft computing based optimization of a novel solar heliostat integrated energy system using artificial neural networks, Sustain. Energy Technol. Assess. 50 (2022), 101850, https://doi.org/10.1016/j.seta.2021.101850.
[32] C. Wang, R. Liu, A. Tang, Energy management strategy of hybrid energy storage system for electric vehicles based on genetic algorithm optimization and temperature effect, J. Energy Storage 51 (2022), 104314, https://doi.org/10.1016/j.est.2022.104314.
[33] A. Izadi, M. Shahafve, P. Ahmadi, Neural network genetic algorithm optimization of a transient hybrid renewable energy system with solar/wind and hydrogen storage system for zero energy buildings at various climate conditions, Energy Convers. Manag. 260 (2022), 115593, https://doi.org/10.1016/j.enconman.2022.115593.
[34] M. Mehrpooya, M. Ashouri, A. Mohammadi, Thermoeconomic analysis and optimization of a regenerative two-stage organic rankine cycle coupled with liquefied natural gas and solar energy, Energy 126 (2017) 899–914, https://doi.org/10.1016/j.energy.2017.03.064.
[35] S. Sadeghi, S. Ghandehariun, G.F. Naterer, Exergoeconomic and multi-objective optimization of a solar thermochemical hydrogen production plant with heat recovery, Energy Convers. Manag. 225 (2020), 113441, https://doi.org/10.1016/j.enconman.2020.113441.
[36] S.M. Alirahmi, A.R. Razmi, A. Arabkoohsar, Comprehensive assessment and multi-objective optimization of a green concept based on a combination of hydrogen and compressed air energy storage (CAES) systems, Renew. Sust. Energ. Rev. 142 (2021), 110850, https://doi.org/10.1016/j.rser.2021.110850.
[37] Y. Li, B. Ming, Q. Huang, Y. Wang, P. Liu, P. Guo, Identifying effective operating rules for large hydro–solar–wind hybrid systems based on an implicit stochastic optimization framework, Energy 245 (2022), 123260, https://doi.org/10.1016/j.energy.2022.123260.
[38] M.A. Behrang, E. Assareh, A. Ghanbarzadeh, A.R. Noghrehabadi, The potential of different artificial neural network (ANN) techniques in daily global solar radiation modeling based on meteorological data, Sol. Energy 84 (2010) 1468–1480, https://doi.org/10.1016/j.solener.2010.05.009.
[39] S. Balafkandeh, S.M.S. Mahmoudi, E. Gholamian, Design and tri-criteria optimization of an MCFC based energy system with hydrogen production and injection: an effort to minimize the carbon emission, Process Saf. Environ. Prot. 166 (2022) 299–309, https://doi.org/10.1016/j.psep.2022.08.020.
[40] A.R. Razmi, S.M. Alirahmi, M.H. Nabat, E. Assareh, M. Shahbakhti, A green hydrogen energy storage concept based on parabolic trough collector and proton exchange membrane electrolyzer/fuel cell: thermodynamic and exergoeconomic analyses with multi-objective optimization, Int. J. Hydrog. Energy (2022), https://doi.org/10.1016/j.ijhydene.2022.03.021.
[41] S.M. Alirahmi, A.R. Razmi, A. Arabkoohsar, Comprehensive assessment and multi-objective optimization of a green concept based on a combination of hydrogen and compressed air energy storage (CAES) systems, Renew. Sust. Energ. Rev. 142 (2021), https://doi.org/10.1016/j.rser.2021.110850.
[42] B. Nourozi, Q. Wang, A. Ploskić, Energy and defrosting contributions of preheating cold supply air in buildings with balanced ventilation, Appl. Therm. Eng. 146 (2019) 180–189, https://doi.org/10.1016/j.applthermaleng.2018.09.118.
[43] E. Gholamian, V. Zare, N. Javani, F. Ranjbar, Dynamic 4E (energy, exergy, economic and environmental) analysis and tri-criteria optimization of a building-integrated plant with latent heat thermal energy storage, Energy Convers. Manag. 267 (2022), 115868, https://doi.org/10.1016/j.enconman.2022.115868.
[44] A. Behzadi, A. Arabkoohsar, Y. Yang, Optimization and dynamic techno-economic analysis of a novel PVT-based smart building energy system, Appl. Therm. Eng. (2020), 115926, https://doi.org/10.1016/j.applthermaleng.2020.115926.
[45] I.B. Mansir, E.H.B. Hani, H. Ayed, C. Diyoke, Dynamic simulation of hydrogen-based zero energy buildings with hydrogen energy storage for various climate conditions, Int. J. Hydrog. Energy (2022), https://doi.org/10.1016/j.ijhydene.2021.12.213.
[46] A. Behzadi, A. Arabkoohsar, V.S. Perić, Innovative hybrid solar-waste designs for cogeneration of heat and power, an effort for achieving maximum efficiency and renewable integration, Appl. Therm. Eng. 190 (2021), https://doi.org/10.1016/j.applthermaleng.2021.116824.
[47] F. Ren, Z. Wei, X. Zhai, Multi-objective optimization and evaluation of hybrid CCHP systems for different building types, Energy 215 (2021), 119096, https://doi.org/10.1016/j.energy.2020.119096.
[48] Sweden Energy Prices, GlobalPetrolPrices.com, 2022. https://www.globalpetrolprices.com/Sweden/. (Accessed 5 July 2022).
[49] Greenhouse Gas Emission Intensity of Electricity Generation in Europe, European Environment Agency, 2022. https://www.eea.europa.eu/data-and-maps/indicators/overview-of-the-electricity-production-3/assessment. (Accessed 28 June 2022).
[50] S. Mirjalili, S. Saremi, S.M. Mirjalili, L.D.S. Coelho, Multi-objective grey wolf optimizer: a novel algorithm for multi-criterion optimization, Expert Syst. Appl. 47 (2016) 106–119, https://doi.org/10.1016/j.eswa.2015.10.039.
[51] T. Azad, in: Implementation of TOPSIS Method for Multi Criteria Decision Making of Supplier Selection, 2019, pp. 22–27.
[52] Sweden's Carbon Tax, Government.se, 2022. https://www.government.se/government-policy/swedens-carbon-tax/swedens-carbon-tax/. (Accessed 28 June 2022).